Energy Conversion and Management 244 (2021) 114491

Contents lists available at ScienceDirect

Energy Conversion and Management

journal homepage: www.elsevier.com/locate/enconman

Pilot-scale biomethanation in a trickle bed reactor: Process performance and microbiome functional reconstruction

Panagiotis Tsapekos [a], Laura Treu [b,*], Stefano Campanaro [b,*], Victor B. Centurion [c], Xinyu Zhu [a], Maria Peprah [a], Zengshuai Zhang [a], Panagiotis G. Kougias [d], Irini Angelidaki [a]

[a] Department of Chemical and Biochemical Engineering, Technical University of Denmark, Kgs., Lyngby DK-2800, Denmark
[b] Department of Biology, University of Padova, Via U. Bassi 58/b, 35121 Padova, Italy
[c] Microbial Resources Division, Research Center for Chemistry, Biology, and Agriculture (CPQBA), State University of Campinas - UNICAMP, Paulínia, SP CEP 13081-970, Brazil
[d] Soil and Water Resources Institute, Hellenic Agricultural Organisation Demeter, Thermi-Thessaloniki 57001, Greece

ARTICLE INFO

Keywords:
Biomethanation
Biogas upgrade
Trickle-bed reactor
Functional metagenomics
Archaea

ABSTRACT

Biogas upgrading is an emerging technology offering unique opportunities for further exploitation of biomethane as fuel for vehicles or direct injection into the gas grid, expanding the conventional use of biogas for combined heat and electricity generation. Up to date, most of the studies exploring the potential of biological carbon dioxide hydrogenation was performed at laboratory scale systems, hampering the evaluation of the process under real environmental conditions. The current work demonstrates the performance of a pilot trickle bed reactor that was fed with real biogas as CO_2 source under progressively increased gas provision rates. Additionally, the study is supported by a genome-centric metagenomic analysis to gain deep insights into the microbiome of the reactor. A maximum methane content of 98.5% was achieved at a gas retention time of 5 h. Stand-by periods in which no influent gas was provided in the reactor did not lead to fatal deterioration of the overall process, as the biomethanation efficiency was recovered after a certain period of time. Samples obtained from three different layers of the packing material, the liquid phase of the reactor and the inoculum demonstrated a distinct clustering of microbial members. The provision of the nutrient media from the top layer led to the enrichment of specific bacteria, such as *Clostridiaceae* DTU-pt_113, whose genome profile contains Veg-family genes, which are known to be associated with biofilm formation. Similarly, the injection of influent gases from the bottom of the reactor favoured the proliferation of hydrogenotrophic methanogens, solely belonging to family *Methanobacteriaceae*.

1. Introduction

With a view of achieving a climate neutral Europe by 2050 and towards deep decarbonisation, European Commission has lately announced the key role of H_2 produced from excess renewables electricity [1]. The surplus electricity, produced from fluctuating renewables during the peak periods, must be consumed to avoid losses or grid congestion [2]. Although the temporary surplus can be partially exported to neighbouring countries, the potential of renewables is not fully utilized. It is anticipated that smart grid approaches should be adopted and effective solutions for storage and utilization of cheap energy should be developed. Hence, excess electricity can be used to produce H_2 appearing as an energy carrier by storing electrons in the form of stable chemical bonds that can be used as a fuel or serve as a carrier to ease Power to X technologies.

Among the conversion technologies for the deployment of H_2 to the energy market, the biological coupling with CO_2 to produce biomethane is a promising alternative [3,4]. Biomethanation can be easily implemented at biogas plants to upcycle the CO_2 in biogas but the current techno-economic metrics (e.g., production capacity, switch on/off flexibility, CAPEX) should be improved to compete with conventional CO_2 capturing technologies (e.g., amine scrubbing, pressure swing adsorption). However, the traditional upgrading processes do not upcycle CO_2 to CH_4 leading to limited environmental benefit and also, at low H_2 prices are less economically advantageous compared to biomethanation [5].

Among the different reactor systems for biomethanation, trickle bed reactor (TBR) appears as an efficient system to achieve high CH_4 quality

* Corresponding authors.
E-mail addresses: laura.treu@unipd.it (L. Treu), stefano.campanaro@unipd.it (S. Campanaro).

https://doi.org/10.1016/j.enconman.2021.114491
Received 11 May 2021; Accepted 29 June 2021
Available online 8 July 2021

and production capacities [6]. In TBRs the microbes can be immobilized on the packing material which should have a high surface-area for gas–liquid mass transfer favouring the high density and activity of methanogenic archaea [7]. Focusing on packing, polyurethane foam is a dense and cheap material posing some characteristics to be used in biological upgrading. Specifically, it was lately associated with high H_2 conversion and CH_4 production rates at lab-test [8]. Despite the promising performance, in the cited study the tests ran only for 60 days and thus, the tolerance of polyurethane against potential operational problems (e.g., filter clogging due to excess biofilm) cannot be concluded.

Considering the exploitation of TBR with different packing materials, long-term pilot experiments were previously conducted. For instance, Strübing et al. [9] operated a pilot-scale TBR that was filled with two different commercially available packing materials for more than 300 days using pure H_2/CO_2 and artificial nutrient media. Subsequently, the same research group followed a more dynamic approach applying a repetitive standby/restart operation (at 25 °C and 55 °C) to evaluate the biomethanation efficiency of a demand/oriented operation [10]. Research showed that the repetitive standby at 55 °C could markedly deteriorate TBR restart due to high inactivation of hydrogenotrophic archaea and volatile fatty acids (VFA) accumulation. However, relatively short standby periods were applied (up to 8 days) at the controlled thermophilic conditions. In contrast, the effect of prolonged standby on TBR restart procedure is not clear and on top of it, the impact of non-controlled temperature has not been evaluated before. Moreover, none of the above-mentioned very informative studies was validated in relevant environments upgrading real biogas and using digestate as a nutrient source.

Apart from reactor design, the microbial species involved in biomethanation markedly determine process efficiency. The microbial community responsible for organic matter to methane conversion is composed of many species and can change in abundance and composition according to the environmental conditions [11]. Revealing the diversity and dynamics of hydrogen-fuelled microbial communities it would be feasible to acquire significant knowledge on how to optimize the operational conditions. Due to the technical difficulties associated with the isolation process of anaerobic microbes, metagenomic approaches are more frequently applied to determine the functional properties of microbes involved in biogas upgrading [12,13]. Methanogenic microbiome is known for its intricate metabolic networks and complex consortium structure. Previous studies showed that the microbiome is typically dominated by uncharacterized species, leading to difficulties on the functional characterization of the key members. Thus, the *de-novo* assembly of individual genomes through genome-centric metagenomics provides significantly deeper insights into the functionality of methanogenic microbes. In addition, the reconstruction of metabolic pathways in metagenome-assembled genomes (MAG) unveiled the potential interspecies interaction among microbes in a methanogenic community [14]. In particular, genome-centric investigations can provide a better characterization of the functional roles of microbial species and more qualitative information in comparison to marker-gene based predictive approaches [15]. Nevertheless, there is scant research on biomethanation reactors operated in relevant environments. Considering that biomethanation will markedly aid the green transition of the bioenergy sector, deeper insights on microbial aspects are needed under more realistic conditions compared to the mainly examined lab-scale trials.

In the present study, the capability of a pilot-scale biomethanation TBR is evaluated using real biogas and digested municipal biowaste as nutrient sources in a relevant environment. The TBR was operated varying the operational conditions and gradually increasing the H_2 feeding rate to assess process performance at long-term. To evaluate process flexibility, the TBR was put twice on standby mode at different temperatures to evaluate restart efficiency. Moreover, microbial samples collected from different heights in the TBR and analysed to reveal microbiome distribution.

2. Materials and methods

2.1. Pilot trickle bed reactor

A trickle bed reactor (TBR) with an overall height of 2.1 m and active filling volume of 68 L was used. The schematic diagram of the TBR and ancillary equipment are depicted in Fig. 1. The reactor shell was constructed of AISI 304 (ø273 × 2 mm; ID 269). The active volume was separated in three sections filled with polyurethane foam which was supported by a polyester grid (h: 25 mm, ø260 mm) to ensure avoidance of packing material displacement.

A screw-in resistance thermometer (JUMO Type PT 100) was placed in the middle of the TBR to monitor and control the temperature at thermophilic conditions (52 ± 1 °C) using a heater cable (Fluoropolymer over jacket over tinned copper braid, EMTS2-CF). Since the process is exothermic, a cooling system was prepared to maintain the temperature of the TBR on the desired level. Hence, when heat was produced as advised by an online thermometer, water at ambient temperature was automatically recirculated using a peristaltic pump (Watson-Marlow, 600 series) through soft copper tubing which was wrapped around the outer surface of the TBR. Inlet and outlet ports were available at the bottom and top layer of the TBR to provide flexibility for either co– or counter-flow operation. The operating pressure was monitored using an analogue positive pressure gauge that was connected to the upper section of the active volume.

Biogas was supplied using a peristaltic pump (Watson-Marlow, 600 series) and hydrogen was provided by a mass flow controller (Bronkhorst High-Tech BV). Gases were injected below the lowest level of TBR's active volume via either craft-made perforated stainless-steel injectors with 5 sets of holes (3 × ø3.5 mm per set) or ceramic membranes made from silicon carbide (SiC) with a 0.5 μm pore size. Sieved digested municipal biowaste was used as a nutrient medium and trickled once per day from the nutrient sump (7.5 L working volume) to the top of the reactor using a peristaltic pump (Watson-Marlow, 600 series). A cylindrical drip tray with multiple drain holes was placed at the top of the reactor to ensure proper distribution of liquid medium.

A pressure relief valve was placed on the top of the TBR for safety. The complete set-up was assembled and installed in a 40-foot container in line with ATEX regulations. All above mentioned electrical and mechanical equipment was connected to an electrical panel and controlled online via LabView (National Instruments, USA).

2.2. Inoculation

A continuously stirred tank reactor (CSTR) with 9.0 L total and 7.5 L working volume was employed to prepare an enriched hydrogenotrophic seed. The CSTR was operated at thermophilic conditions (52 ± 1 °C), the typical operation for biogas plants in Denmark, using a silicone thermal jacket and was further used in the pilot test as nutrients sump (Fig. 1). For inoculum preparation, the working volume of the CSTR consisted of 90% with the effluent of a pilot-scale biogas reactor (working volume: 500 L) fed with municipal biowaste and 10% with hydrogenotrophic inoculum derived from a lab-scale upgrading reactor [16]. The municipal biowaste was pretreated in a pulping facility [17] and then, was anaerobically digested at a hydraulic retention time of 20 days under mesophilic conditions. The raw municipal biowaste had the following characteristics (g/kg): 166.34 ± 36.49 total solids (TS), 140.16 ± 28.84 volatile solids (VS), 4.27 ± 0.98 total nitrogen (TN), 0.76 ± 0.20, ammonium nitrogen (NH_4-N) and 4.4 pH. The effluent of the biogas reactor was collected in storage tanks and before usage, it was sieved and filtered to avoid operational problems and clogging during trickling. The finally used digested municipal waste had the following characteristics (g/kg): 14.23 ± 1.85 TS, 9.94 ± 1.36 VS, 1.09 ± 0.09 NH_4-N, and 7.09 pH. The content of essential trace elements (i.e. Fe, Ni, Co) for methanogenesis was also defined and is presented below.

The CSTR was flushed with an 80:20 (v/v) mixture of H_2 and CO_2,

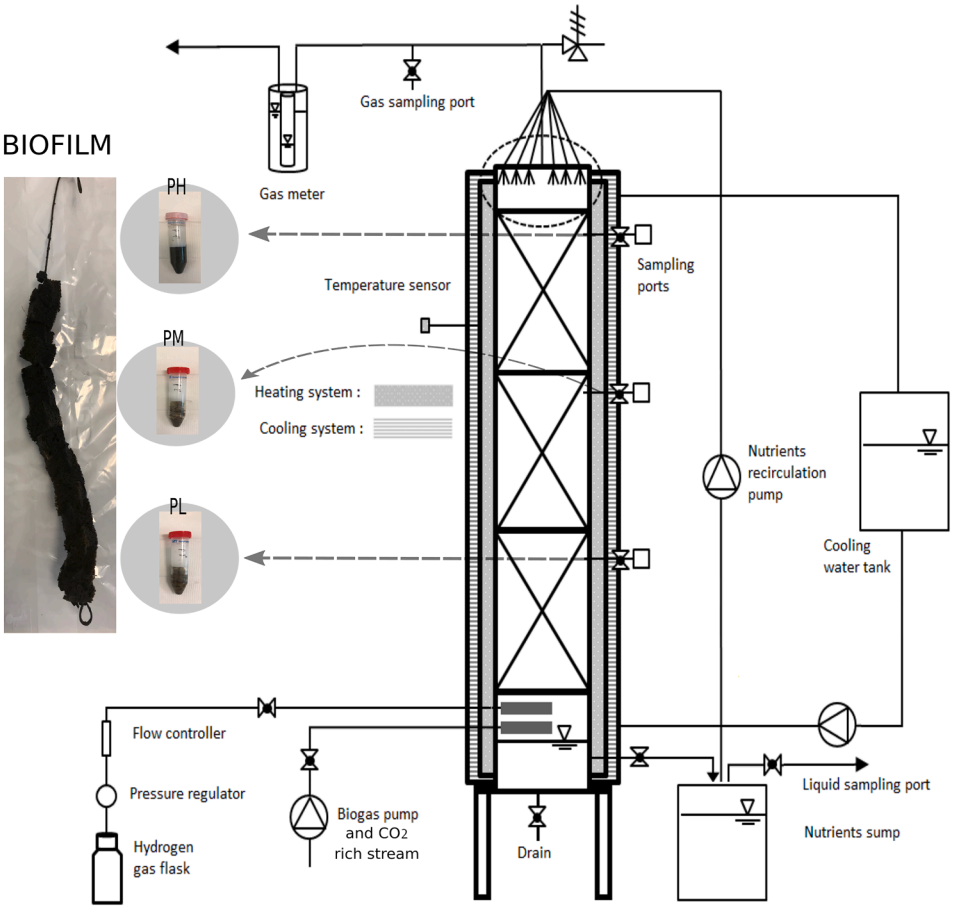

Fig. 1. Schematic diagram of the pilot-scale trickle bed reactor. Gray dashed arrow represents the points of sampling and biofilm appearance. **PL**: low point; **PM**: middle point; **PH**: high point.

while a gasbag filled with the same gas feedstock was connected at the headspace. The gas was continuously circulated using a peristaltic pump and injected into the working volume using a ceramic diffuser. Due to H_2 and CO_2 coupling a pressure drop appeared and fresh gas feedstock was daily added. During the cultivation period, 10% of liquid volume was replaced twice a week to ensure adequate nutrients provision. The CSTR was operated for one month and subsequently, the enriched hydrogenotrophic culture was used to inoculate the pilot TBR. Prior to TBR start-up, 40 L of sieved digested biowaste was continuously trickled to ensure wetting of packing material and ease microbial access to nutrients. Then, the 7.5 L of enriched inoculum was loaded into the upper surface of the TBR.

2.3. Operating conditions and monitoring

The TBR was flushed with N_2 for 30 min before start-up to ensure anaerobic conditions. During the first 8 days (P-1), the H_2:CO_2 feedstock was settled to a 2:1 ratio to avoid H_2 overfeeding and rapid pH increase. Subsequently, the feedstock was adjusted to the stoichiometrically needed 4:1 up to day 27 reaching a gas retention time (GRT) of 10 h (P-2). To evaluate the effect of "hot standby" period (i.e., no feeding and keeping unchanged the temperature) [6], the gas provision was ceased from day 28 to day 53 (P-3). Then, the TBR was fed again at the same feed rate (P-4). The gas feeding rate was increased again at day 81 to reach a 5 h GRT (P-5) and at day 110 the craft-made perforated stainless-steel injectors were replaced with Sic membrane as means to improve H_2 diffusion (P-6). The operational conditions were kept unchanged up to day 118. Then, a "cold standby" period (i.e., no feeding and ambient temperature) was established for 75 days (P-7). The TBR was restarted at day 234 using biogas as CO_2 source and operated at 10 h GRT up to day 256 (P-8). Then, the GRT was adjusted to 5 h (P-9) and finally, the TBR was operated at 2 h GRT (P-10). The detailed plan of the operating conditions is presented in Table 1 and the GRT was calculated based on reactor volume (V_{TBR}) and the total feeding gas (F_{in}), as shown in Eq. (1).

$$GRT = \frac{V_{TBR}}{F_{in}} \quad (1)$$

From day 0 to 193, the container with the integrated TBR unit was placed in BIOFOS WWTP (Avedøre, DK) and was fed with a mixture of CH_4/CO_2 at 60/40 (v/v) as an artificial biogas (Air Liquide A/S, Denmark). At the end of the second standby period (day 194), the unit was operated at Lemvig Biogas (Midtjylland, DK) and fed with biogas produced in the plant derived after desulfurization. Microaerobic removal of H_2S is applied in the biogas plant and thus, residual O_2 (<0.2 vol%, monitored as safety limit) could be occasionally available on the outlet side of the biological process. CH_4 and CO_2 content in the biogas was regularly defined to adjust the value of added H_2. During the whole experimental period pure H_2 was used (ALPHAGAZ™ 1 $H_2 \geq$ 99.999 mol%, Airliquide) and digested municipal biowaste was utilized as a nutrients source. Before usage, the digestate was sieved to remove large particles that could provoke clogging. Apart from standby periods, the nutrient solution was trickled once per day at a rate of 1.2 L/min and allowed to drain by gravity to return to the sump. Changes of the gas feed rate, temperature variation and operation/standby periods throughout the entire experiment are depicted listed in Fig. 2.

Table 1
Operating conditions and characteristics.

Period	Days	T (°C)	H_2: CO_2	CO_2 source	F_{in} (L/day)	GRT (h)	Gas dispersion system	Notes
1	0–8	52 ± 1	2:1	Pure	115	14	Craft-made perforated stainless-steel injectors with 5 sets of holes (3 × ø3.5 mm per set)	
2	9–27		4:1		163	10		
3	28–53	52 ± 1	–	–				"hot standby" period
4	54–80	52 ± 1	4:1	Pure	163	10		
5	81–109	52 ± 1	4:1	Pure	327	5		
6	110–118	52 ± 1	4:1	Pure	327	5	Ceramic membranes made from silicon carbide (SiC) with a 0.5 μm pore size.	
7	119–193	Ambient	–	–	327	–		"cold standby" period
8	194–233	52 ± 1	4:1	Biogas	163	10		
9	234–256	52 ± 1	4:1	Biogas	327	5		
10	255–276	52 ± 1	4:1	Biogas	817	2		

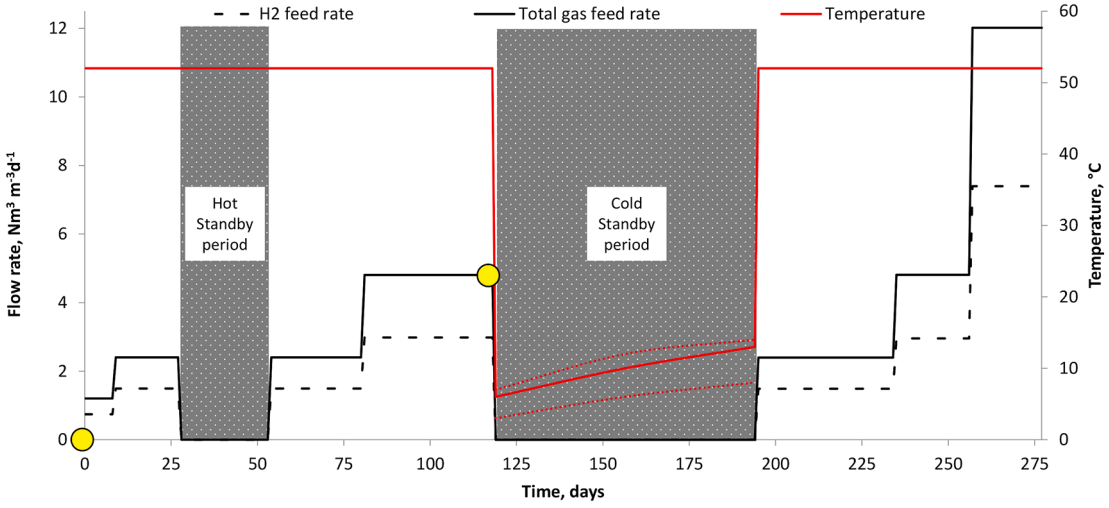

Fig. 2. Simplified operational scheme indicating the operational and standby periods and the corresponding reactor temperatures lower and upper, H_2 and total gas feed rates. Yellow circles represent the sampling dates for DNA extraction. In the cold standby period, the dashed red lines depict the minimum and maximum ambient temperatures, while the straight line stands for the average.

2.4. Analytical methods and data analysis

The standard methods for the examination of water and wastewater were followed to measure TS, VS, pH, and ammonium nitrogen (NH_4-N) [18]. The VFA composition was determined using a GC-TRACE 1300 (Thermo Scientific) as previously described by Khoshnevisan et al. (2018a). The effluent gas was quantified using the water displacement method. Gas samples were daily collected in vacuum vials (Exetainer® 5.9 mL Evacuated Flat Bottom Vial) to monitor the biomethanation efficiency. A gas chromatograph GC-TRACE 1310 (Thermo Scientific) was used to determine the methane content and production capacity. All measurements were measured in duplicate and results significance ($p < 0.05$) was defined by analyses of variance (ANOVAs) and Student's *t*-test using the OriginPro 9.0.0 SR2 software (OriginLab Corporation, USA).

2.5. Microbial sampling and DNA extraction

To explore the microbial diversity and dynamicity along the TBR height, three samples for genomic DNA extraction were collected from the high, middle, and low points of the filter (PH, PM, and PL, respectively). Moreover, liquid sample (Li) was also extracted from the nutrients sump to define the planktonic microbiome, and inoculum microbiome was also characterized. Hence, five samples were analysed in total, including the inoculum sample (In). The samples from the TBR were collected at day 118 and used for metagenomic analysis. Genomic DNA extraction was performed using DNeasy PowerSoil® (QIAGEN GmbH, Hilden, Germany) with minor modifications as previously described [16]; an initial cleaning step with Phenol:Chloroform: Isoamyl Alcohol (25: 24: 1) was implemented to increase the purity of the extracted nucleic acids. Quality control on extracted DNA was done by means of NanoDrop (Thermo Fisher Scientific, Waltham, MA, USA) for purity and Qubit (Thermo Fisher Scientific, Waltham, MA, USA) for concentration.

2.6. Metagenomic sequencing and binning analysis

Library preparation was performed using the Nextera DNA Flex Library Prep Kit (Illumina Inc., San Diego CA) and sequenced with the Illumina NovaSeq 6000 platform (2 × 150, paired end) at the CRIBI Biotechnology Center sequencing facility (University of Padova, Italy). Raw sequences were uploaded to the Sequence Read Archive (NCBI) under the project ID PRJNA694528.

Reads were filtered using Trimmomatic v 0.39–1 tool [19] to remove adapters and trim out low-quality bases (Phred score ≤ 20). BBDuck software (BBTools, jgi.doe.gov/data-and-tools/bbtools) was used for eliminating bacteriophage phi X 174 contamination sequences. Co-assembly was carried out using MegaHit (v1.2.9) tool [20] with "meta-large" option. Contigs shorter than 1 kbp rarely encode complete genes and they provide little information on gene functions, for this reason they were removed. Bowtie2 (v2.2.6) [21] and SAMTool (v.1.10) [22] were used to generate the contigs coverage profiles for the subsequent binning approach. Metagenome Assembled Genomes (MAGs)

were identified with MetaBAT2 (v2.12.1) [23]. CheckM (v1.1.2–1) [24] was used to assess quality (completeness and contamination) and relative abundance of the MAGs in each sample. MAGs were classified as high quality (≥90% completeness, ≤ 5% contamination), medium quality (≥50% completeness, ≤ 10% contamination), low quality (≤50% completeness, ≤ 10% contamination), and bad quality (>10% contamination). The taxonomic classification of the MAGs was made by GTDB-Tk (v1.0.2) [25]. Finally, the prediction of protein encoding genes in each MAG was performed with Prodigal (v2.6.3) [26]. Genes functional annotation and functional investigation was performed with DRAM (v1.1.1) [27] and EggNOG (v5.0) tools [28].

2.7. Statistics and data visualization

MAGs relative abundance was visualized as heatmap using R (v3.6.3) (R core team, 2020) and the heatmaps of heatmaply (v1.1.1) package [29]. MAGs distribution in samples was checked using the Principal Component Analysis (PCA) of vegan (v2.5–6) package [30]. Out of the DRAM tool results, only the Kyoto Encyclopedia of Gene and Genomes (KEGG) module database [31] and pathways of importance for biogas production were selected and visualized as heatmaps with ggplot2 (v3.3.2) package [32]. Manual investigation of specific KEGG IDs was performed by colouring the genes in the pathway maps using KEGG mapper, and the metabolic reconstruction of MAGs was visually represented with BioRender (https://biorender.com/). Identification of genomes belonging to the same MAGs previously reported was performed with Average Nucleotide Identity calculation in the MiGA platform [33] using as reference the Bio-Gas microbiome database.

3. Results and discussion

3.1. Bioconversion of H_2 and CO_2 to CH_4

High biomethanation efficiency was achieved since the first week of operation reaching more than 90% in the output (Fig. 3a). After feed regime adjustment at the stoichiometrically optimum at day 8, a slight drop of upgraded methane was detected from day 10 to 18. However, at the end of P-2 and prior to "hot standby" period, no residual H_2 was detected in the output, and the CH_4 content was equal to 90%.

A remarkably high CH_4 concentration (98%) was detected at P-4. A deviation to the H_2 flow was faced from day 72 to 75 reducing the upgrading efficiency. Once the H_2 flow was adjusted to the correct value, the biomethane content reached again more than 95%. The lowering of the GRT at 5 h (P-5) by doubling the feeding load affected negatively the biomethanation performance. Specifically, the CH_4 was decreased to 58% after 4 days of operation and stabilized to 76% at day 110. In parallel, a slight pH drop and acetate accumulation was observed, suggesting the presence of homo-acetogenic bacteria (Fig. 3b). Via the Wood-Ljungdahl, the homo-acetogens convert CO_2 to acetate causing pH decrease. In accordance, a recent study in an up-flow biomethanation reactor filled with packing material found that the partial utilization of CO_2 and H_2 for homo-acetogenesis instead of methanogenesis led to pH reduction [34].

Another factor that might affected negatively the biomethanation process is the concentration of micronutrients that were found to be significantly decreased during P5. Micronutrients, such as Ni, Co and Fe, are essential for basal microbial functions. It is well known that hydrogenases are Ni-Fe enzymes and efficient cytochromes biosynthesis requires iron within a defined concentration range. Additionally, it has been previously reported that low content of micronutrients has a detrimental role on the methanogenic activity of anaerobic biofilms [35]. In the current experiment, the concentrations of Co and Ni were significantly lower (6 and 10 μM, respectively) at the beginning of P-5 (day 80) compared to the beginning of the test (21 and 37 μM, respectively) to. In accordance with the current work, the limited ability of archaea to perform a high biomethanation rate along with VFA accumulation was previously revealed due to shortage of Co and Ni [36]. Similarly, the concentration of Fe in the nutrients' sump was also reduced from 302 to 51 μM compared to day 0 (Table 2). Based on literature, the optimal levels for Ni and Fe for hydrogenotrophic methanogenesis are 0.2–1 and 15–500 μM, respectively [37]. Considering that the micronutrient concentration was above the literature threshold levels, even though they were found to be decreased, the strategy on nutrients provision did not change through the experiment. Thus, it was hypothesized that the limited biomethanation efficiency could be attributed to the fact that polyurethane foam was very thick filling material, and for these reasons the contact between nutrients and gases was not optimized leading to a non-homogenous biofilm creation

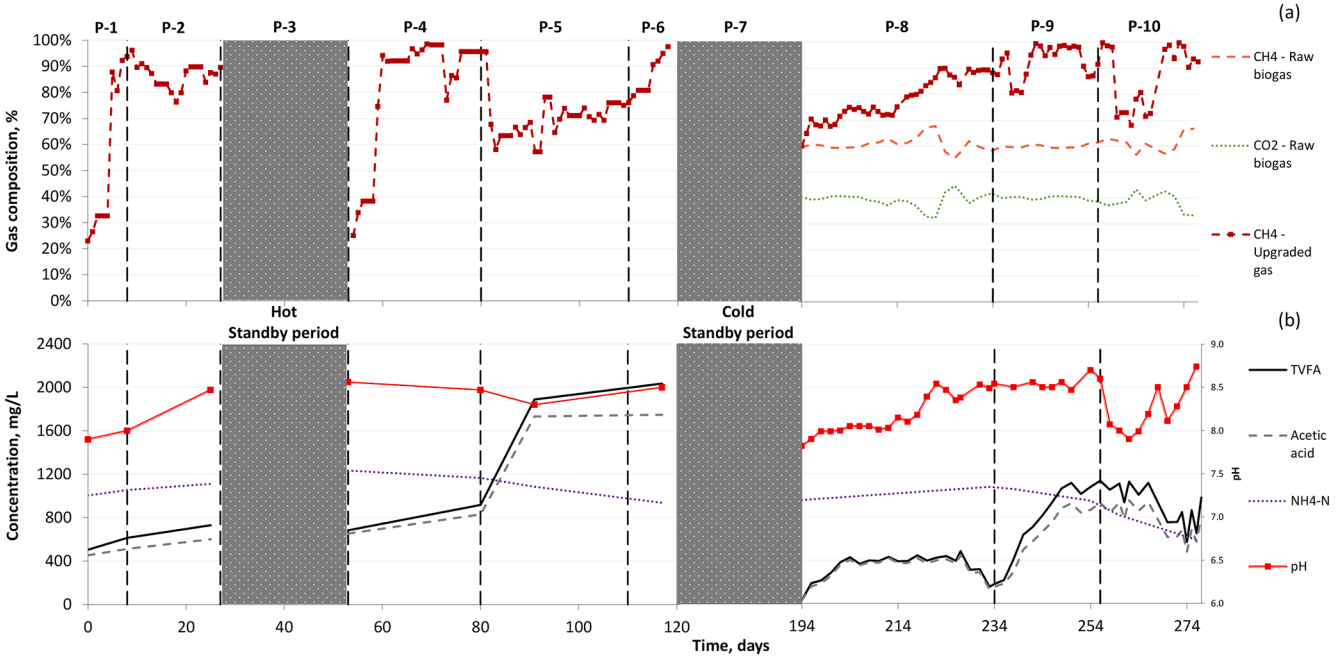

Fig. 3. Biomethane content (a), TVFA and acetic acid accumulation, NH_4-N and pH fluctuation (b) of TBR.

Table 2
Content of crucial trace elements for enzymatic activity of methanogenic archaea.

Day	Fe, μM	Co, μM	Ni, μM
0	302	21	37
53	54	6	11
80	51	6	10
117	37	4	8
194	42	6	10
234	31	5	9
256	43	8	12
276	53	10	16

throughout the TBR bed. This hypothesis was validated during sample collection for microbiological analysis showing thicker biofilm formation at the top of the TBR, the position from where the nutrients were trickled (Fig. 1). To overcome limited biomethanation, the perforated stainless-steel injectors were replaced with SiC membrane at day 110 as means to improve the gas–liquid contact. Indeed, the positive impact was quickly revealed and biomethane content reached a value of 98% at day 110. In parallel, the acetate levels were not significantly increased (from 1732 to 1747 mg/L, $p > 0.05$), validating the improved hydrogenotrophic activity compared to the previous period.

Subsequently, the "cold standby" followed, and after 75 days at ambient temperature, the TBR initiated at 10 h GRT using real biogas. A small leakage did not allow proper H_2 provision, and thus, almost 30 days were needed to adjust the feeding regime at the appropriate stoichiometry. Once the problem was fixed, more than 90% CH_4 was achieved similarly to the previous experimental period at 10 h GRT. Subsequently, by further increasing the feeding rate (P-9, GRT: 5 h) more than 98.5% CH_4 content was observed which was the superior upgrading efficiency during the whole experiment. Finally, by adjusting the feeding rate to the highest value, i.e., GRT: 2 h at P-10 a clear drop on biomethanation efficiency was detected, along with a concomitant drop in pH values below 8.0. This can be explained as the partial CO_2 pressure is in balance with the dissolved H_2CO_3 and the pH fluctuation is the result of a bicarbonate buffer system. During efficient hydrogenotrophic methanogenesis, CO_2 is coupled with H_2 and the increased pH favours HCO_3^- formation as shown in Eq. (2), while Eq. (3) is mainly favoured above pH of 10.

$$H_2CO_3 \rightarrow HCO_3^- + H^+ \quad (2)$$

$$HCO_3\text{-} \leftrightarrow CO_3^{2-} + H^+ \quad (3)$$

Nevertheless, the CO_2 uptake rate is enhanced at alkaline conditions. In accordance, the upgrading efficiency increased to the highest standards (>95% CH_4) when the pH increased to similar levels as before and the major dissociated form of CO_2 was HCO_3^-. Despite optimal range for AD process is considered from 7.0 to 8.0, the ex-situ methanogenesis typically occurs in a more alkaline environment due to external H_2 provision and CO_2 uptake. Ashraf et al. found that the production capacity of TBR was not decreased even at pH values higher than 8.5 showing tolerance of the community at more alkaline conditions [38]. In the present study, the H_2/CO_2 fueled microbiome was also efficiently functioning at such pH levels.

3.2. Microbiome in biogas upgrading TBR

3.2.1. General microbial community profile

The genome-centric metagenomic analysis applied to all microbial samples generated 191 MAGs out of which 48 were of high quality and 75 of medium quality. Only the MAGs with high and medium quality (n = 123) were retained for further analyses, such as statistics and bioinformatics functional investigation. According to the percentage of mapped reads (66 to 75% depending on the sample), the selected MAGs accounted for more than half of the total community. The global microbiome heatmap coverage shows nearly identical profiles of samples PL and PM (Supplementary Fig. 1), highlighting that the communities present in the medium–low part of the reactor were highly homogeneous. On the contrary, the remaining samples (In, Li, and PH) had clearly distinct profiles and clustered individually. *Firmicutes* (n = 81) was the dominant phylum in all the samples and was represented mainly by members of the class *Clostridia* (n = 37) (Supplementary Table 1). *Bacteroidetes* (n = 15) and *Proteobacteria* (n = 11) were the second and third most presented phyla, respectively. The methanogenic archaea were represented by three MAGs assigned to the *Methanobacteriaceae* family (*Methanothermobacter wolfeii* DTU-pt_43, *Methanobacterium* DTU-pt_46, *Methanobacteriaceae* DTU-pt_063). For the sake of clarity, only the ten more abundant MAGs of each sample were selected and visualized in the heatmap (Fig. 4a). *Clostridia* DTU-pt_99 was dominant in the inoculum (25%) and it was the third most abundant (6%) in the planktonic sample, followed by *Firmicutes* DTU-pt_168 and *Chromatiales* DTU-pt_172 (both at 11%). Consequently, *Clostridia* DTU-pt_99 was the main responsible for the bioprocess occurring in In and Li samples (Fig. 4b). On the contrary, *Clostridiaceae* DTU-pt_113 was the dominant microorganism (19%) in the PH sample, clearly demonstrating a stratification of microbial members throughout the length of the TBR. *Methanobacterium* DTU-pt_46 was the dominant microorganism in the samples PL and PM, (20%) and the only MAG clearly associated with the medium–low part of the reactor, thus the main methanogen of the whole system. The other two identified methanogens were found in significantly lower relative abundance; specifically, *Methanothermobacter wolfeii* DTU-pt_43 was the second most abundant (0.8% average), while the abundance of *Methanobacteriaceae* DTU-pt_063 was less than the minimal threshold considered. Focusing on *Methanothermobacter* spp., their ability to efficiently form biofilm on ceramic packing materials and then, couple H_2 and CO_2 for CH_4 production was lately revealed [39]. Nevertheless, this recent study followed a pure culture gas fermentation which can be more susceptible to process disturbances compared to the mixed culture of the present study. Moreover, *Methanothermobacter* spp. were also found to dominate the biogas upgrading community in up-flow system equipped with ceramic membranes [40].

The 35 most abundant MAGs have, in general, the potential to degrade carbohydrate through pentose phosphate, Emden-Meyerhof (EM), Wood-Ljungdahl (WL) pathways and citrate cycles (Fig. 5a) and, consequently, to produce acetate and acetyl-CoA (Fig. 5b). The metabolic annotation revealed a high abundance of putative homoacetogenic bacteria (e.g., DTU-pt_99 and DTU-pt_113), which can use H_2 and CO_2 and produce acetate through the WL pathway (Supplementary Table 2). Despite difficulties in correlating gene content with acetogenic behaviour, this finding, obtained from functional annotation, is a possible explanation for the acetate accumulation (1747.81 mg/L) observed after 80 days of operation (Fig. 3b). The high abundance of these bacteria agrees with previous findings in reactors fed with H_2 and CO_2, and a syntrophic relationship with methanogenic archaea was previously hypothesized [41,42]. The three most abundant MAGs present in the planktonic sample (DTU-pt_99, DTU-pt_168 and DTU-pt_172) have similar metabolic pathways, and this suggests a shared functional behaviour. The only difference is in the Cytochrome complex, which is complete in *Chromatiales* DTU-pt_172, a purple sulfur bacteria of the class *Gammaproteobacteria* characterized by reduced sulphur compounds as electron donors [43].

To overcome the issue derived for incomplete MAG genomes, the most relevant MAGs identified according to PCA analysis (Fig. 4b) with values lower than 90% were compared with the MiGA Bio-Gas Microbiome database through ANI analysis. *Clostridia* DTU-pt_99 and *Clostridiaceae* DTU-pt_113 have high similarity with *Firmicutes* sp. AS24abBPME_73 (99% ANI, 98.1% of completeness) and *Clostridia* sp. AS23ysBPME_31 (98% ANI, 56.6% of completeness), respectively. Thus, the more complete reference genome was used to reconstruct the metabolic pathway (Fig. 6); this was done under the assumption that

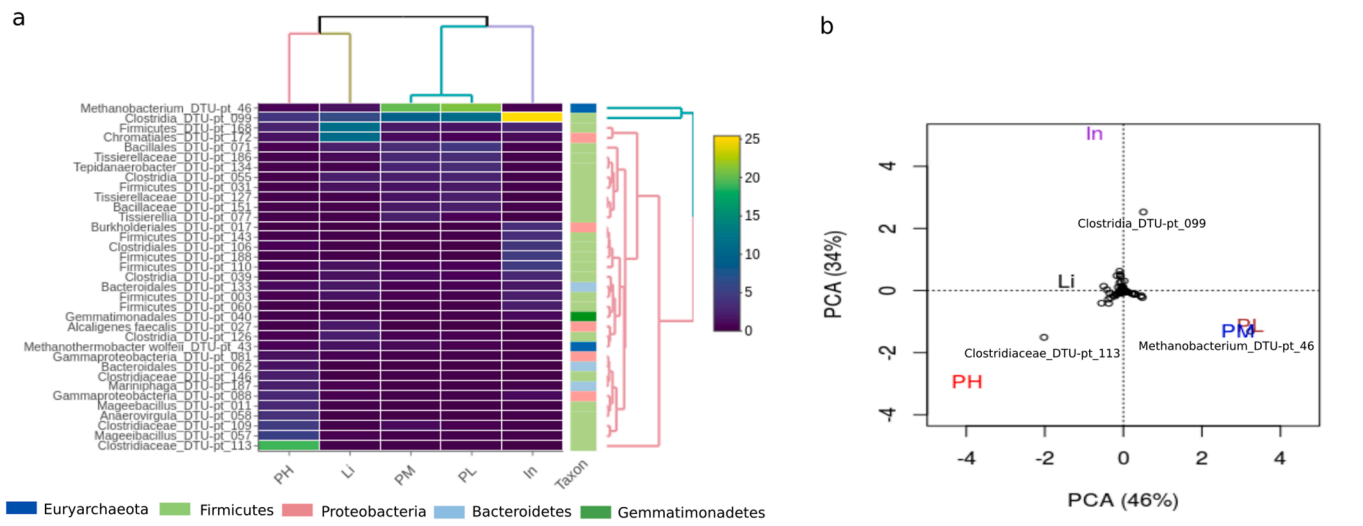

Fig. 4. Selected MAGs abundance and distribution. (a) Heatmap of 35 high abundant MAGs. The taxon colors are the information of phylum level. (b) Principal component analysis (PCA) of the different samples and MAGs. **In**: Inoculum; **Li**: Liquid; **PL**: low point; **PM**: middle point; **PH**: high point.

MAGs having high similarity at genome level were also sharing most functional pathways.

3.2.2. *Microbial spatial stratification*

As previously mentioned, the microbial community structure was divided in distinct clusters within the TBR. The microbial spatial stratification was attributed to two main factors as a result of the process operation. The first factor is associated with the nutrient provision that was facilitated from the top of the reactor enabling the formation of a thick biofilm with high affinity at the upper part of the packing material. The biofilm was getting progressively thinner while moving to the lower parts of the packing material. This observation is aligned and supported with the abundance profile of *Clostridiaceae* DTU-pt_113 which was found to be greater enriched in PH samples rather than in PM and PL samples (Fig. 4). The sequenced data identified the presence of the gene family VEG (PF06257), which is associated with biofilm formation, in the genome of *Clostridiaceae* DTU-pt_113. More specifically, this family is highly conserved in gram-positive bacteria and has the function of stimulating the production of the amyloid fibre component of the biofilm [44]. The second factor for the spatial stratification was attributed to the provision of H_2 and CO_2, which were both injected from the lower part of the reactor. Such environmental conditions favoured the proliferation of methanogens especially at PL and further to PM samples indicating that methane was produced, mainly, in the low and middle points of the TBR (Fig. 4). It was found that methanogenesis was accomplished mainly by *Methanobacterium* DTU-pt_46; in fact, the taxonomic classification agreed with the presence of the complete pathway of hydrogenotrophic methane production identified in the genome of this MAG (Fig. 6). It must be noted that another microorganism with high relative abundance in PL and PM samples was *Clostridiaceae* DTU-pt_99. This MAG was the dominant microbial member in inoculum (In) and it would have been expected that its abundance would remain stable independently from the sampling point. Nonetheless, as shown in Fig. 4, the coverage profile of *Clostridiaceae* DTU-pt_99 was correlated with the corresponding one of *Methanobacterium* DTU-pt_46, suggesting a putative syntrophic relationship due to this frequent co-occurrence. In fact, *Clostridiaceae* DTU-pt_99 belongs to the same species of unclassified Bacteria sp. DTU645 (>99.5% ANI) that was dominant in the microbiome together with several hydrogenotrophic archaea [45]. It has been previously reported that this bacterium performs an alternative pathway for acetate degradation to CO_2 through reversed glycine reduction [45].

Based on the thermodynamics, the hydrogenotrophic methanogenesis and homo-acetogenesis are more energetically favorable compared to acetate oxidation at areas close to H_2 supply and proximity [46]. Thus, it is expected that the H_2 is locally utilized for these two processes, while syntrophic acetogenesis and homo-acetogenic oxidation can occur in areas with lower H_2 availability. At a micro-scale methanogenic membrane reactor, it was found that hydrogenotrophic methanogenic biofilm was located above the gas permeable membrane while the syntrophic acetogens and homo-acetogenic oxidizers were mainly functional in the bulk phase away from the H_2 supplementation area [47]. In a higher scale, a similar stratification was observed herein. The relative abundance of hydrogenotrophic methanogens was markedly high in the zones close to the added H_2 (samples PL and PM), while potential homo-acetogens (*Clostridiales* DTU-pt_099) were also detected in these samples. On the other hand, acetogenic *Clostridiaceae* DTU-pt_113 were found in the upper zone of the TBR where the available H_2 was significantly lower than the middle and low zones. As mentioned above, the utilized packing material did not allow a proper gas distribution and nutrients trickling through reactor bed. To improve the homogeneity of microbial distribution, alternative packing materials of high surface area and porosity could be helpful. In addition, continuous trickling can contribute on higher nutrient availability compared to the applied once per day trickling. However, high trickling rates can allocate the packing materials and vigorously mix the community interrupting the syntrophic associations which are important for mixed fermentation as shown in different reactor systems [48]. On the other hand, absence of mixing can clearly lead to stratification of full-scale digesters [49]. Thus, a continuously slow trickling rate can be beneficial for biomethanation ensuring nutrients availability and decreasing stratification.

3.3. *Future perspective*

Microbial analysis showed that the native AD microbiome can be naturally reconstructed and form a highly efficient community able to operate with raw biogas and nutrients from the digestate. The outcome of this study is particularly important showing that the suggested technology offers an alternative to other industrial upgrading processes relying on single-celled methanogenic archaea as biocatalyst and pure media for nutrients provision. Considering that the present study demonstrated biomethanation using a pilot-scale reactor at relevant environment, system analysis of the whole concept should be now conducted. The feasibility of biomethanation compared to conventional methods for biogas cleaning (i.e., water and amine scrubbing) should be

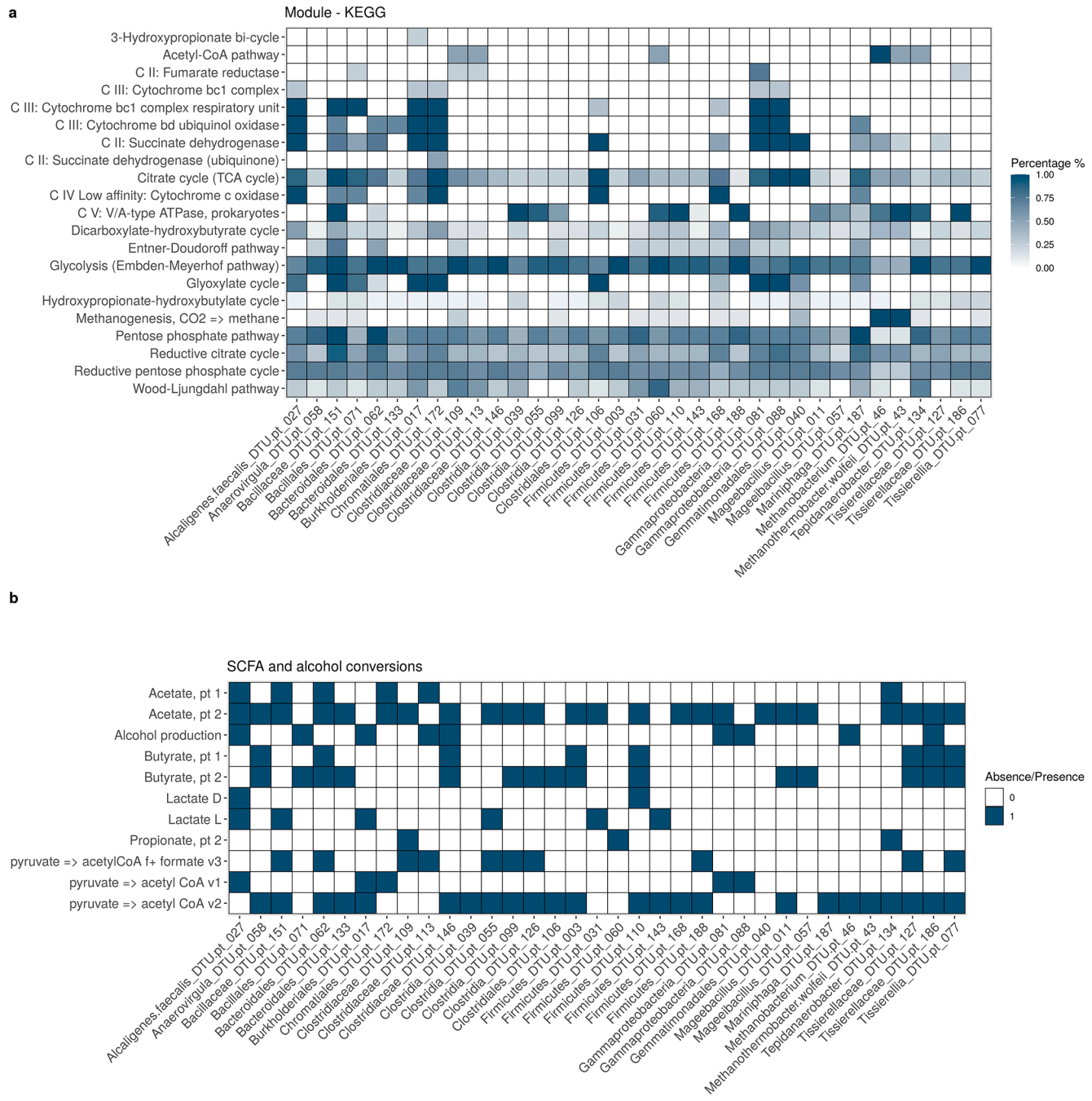

Fig. 5. Heatmap of DRAM results for 35 highly abundant MAGs. (a) Completeness level of KEGG modules functions is reported as percentage. (b) Short-chain fatty acid (SCFA) and alcohol conversion functions are reported as absent ("0" - white) and present ("1" - blue).

evaluated. Since CO_2 is biologically upcycled in the existing technology to produce more energy, a more environmentally friendly approach is achieved. This advantage must be confirmed via detailed techno-economic assessment which can also help the further up-scaling to industrial applications. Finally, business plan can further help to reveal the need for different kinds of subsidies and incentives to increase feasibility of the developed biomethanation technology. When sustainability is validated, biomethanation can be further exploited in other industries as for example fermentation sites, biorefineries, cement, and lime industries to capture the produced CO_2. The potential usage of the native AD microbiome in TBR will allow carbon-intensive industries to improve environmental footprint, enhance productivity and profitability. Biomethanation can be a significant contributor to the green transition.

4. Conclusions

The current work evaluated for the first time the process performance and the microbial spatial distribution of a pilot trickled bed reactor for biomethanation using real biogas as CO_2 source. Maximum biomethanation efficiency led to an output gas with a methane content of 98.5%. Additionally, genome-centric metagenomics revealed a strong stratification of the microbial community which is coherent with the metabolic functions occurring in different layers. Methanogens and potential syntrophic bacteria proliferated close to the influent gas injection ports. On the contrary, microbes whose genome profile contains genes associated with biofilm formation and stimulation dominated the upper layer of the packing material, most probably due to the rich-nutrient media that was trickling from the top of the reactor. The

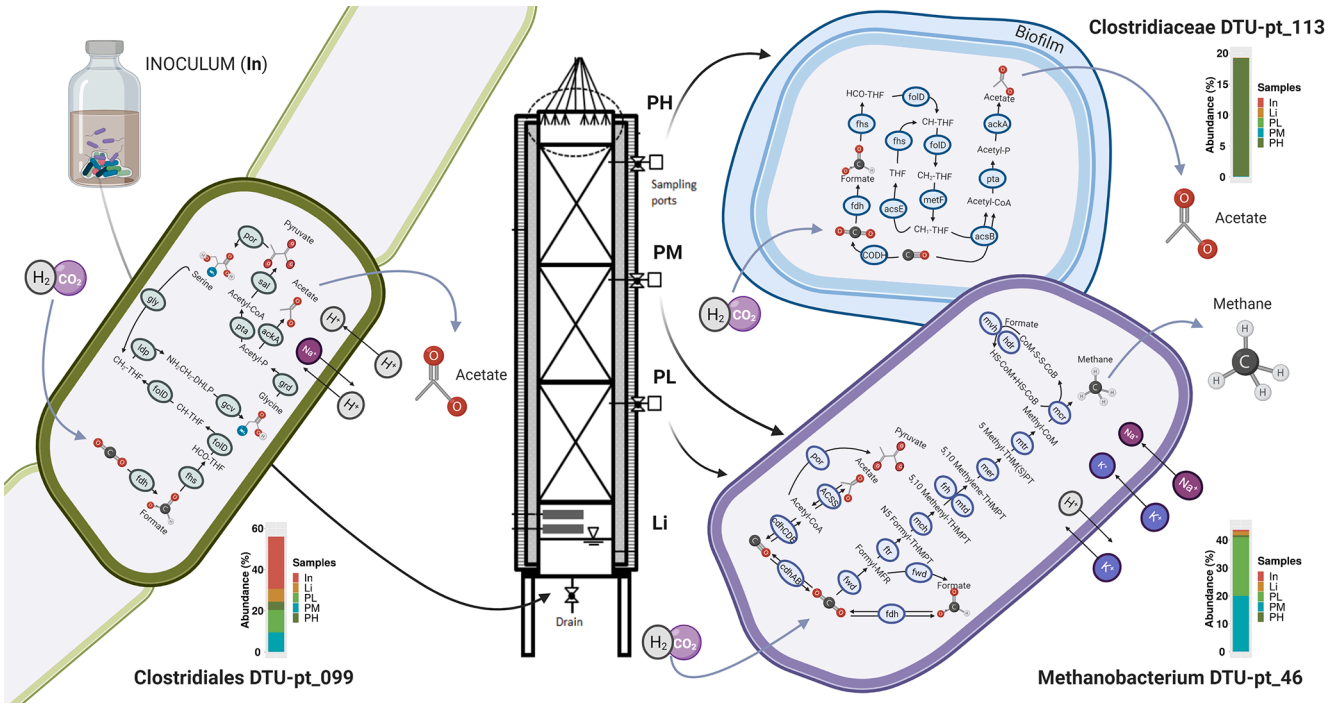

Fig. 6. Metabolic reconstruction of three selected MAGs based on results obtained from KEGG database. The cells represent the H_2 and CO_2 utilization pathways for the production of acetate (green color: WL pathway incomplete, blue color: WL pathway complete) and methane (purple color). Histograms represent the selected MAGs abundance in each sample. **In**: Inoculum; **Li**: Liquid; **PL**: low point; **PM**: middle point; **PH**: high point.

results from the current work are essential and can be directly exploited for elevating the technological maturity of biological biogas upgrading process.

CRediT authorship contribution statement

Panagiotis Tsapekos: Investigation, Data curation, Visualization, Writing – original draft. **Laura Treu:** Data curation, Supervision, Writing – review & editing. **Stefano Campanaro:** Resources, Writing – review & editing. **Victor B. Centurion:** Software, Methodology, Data curation, Writing – original draft. **Xinyu Zhu:** Investigation, Writing – review & editing. **Maria Peprah:** Investigation, Methodology, Data curation. **Zengshuai Zhang:** Investigation, Methodology, Data curation. **Panagiotis G. Kougias:** Conceptualization, Data curation, Writing – review & editing. **Irini Angelidaki:** Funding acquisition, Resources, Conceptualization, Methodology, Writing – review & editing.

Declaration of Competing Interest

The authors declare that they have no known competing financial interests or personal relationships that could have appeared to influence the work reported in this paper.

Acknowledgements

We acknowledge financial support from projects BioUpgrade (ForskEL 2016-1-12465), eFUEL (EUDP 64018-0559), VARGA (MST-141-01377), FUBAF (MST-117-00508) and São Paulo Research Foundation - FAPESP (Process no. 2019/22891-0).

Appendix A. Supplementary data

Supplementary data to this article can be found online at https://doi.org/10.1016/j.enconman.2021.114491.

References

[1] Communication COM/2020/301: A hydrogen strategy for a climate-neutral Europe | Knowledge for policy n.d. https://knowledge4policy.ec.europa.eu/publication/communication-com2020301-hydrogen-strategy-climate-neutral-europe_en (accessed January 21, 2021).
[2] Szima S, Nazir SM, Cloete S, Amini S, Fogarasi S, Cormos A-M, et al. Gas switching reforming for flexible power and hydrogen production to balance variable renewables. Renew Sustain Energy Rev 2019;110:207–19. https://doi.org/10.1016/j.rser.2019.03.061.
[3] Angelidaki I, Treu L, Tsapekos P, Luo G, Campanaro S, Wenzel H, et al. Biogas upgrading and utilization: Current status and perspectives. Biotechnol Adv 2018;36:452–66.
[4] Alibardi L, Green K, Favaro L, Vale P, Soares A, Cartmell E, et al. Performance and stability of sewage sludge digestion under CO_2 enrichment: A pilot study. Bioresour Technol 2017;245:581–9. https://doi.org/10.1016/j.biortech.2017.08.071.
[5] Vo TTQ, Wall DM, Ring D, Rajendran K, Murphy JD. Techno-economic analysis of biogas upgrading via amine scrubber, carbon capture and ex-situ methanation. Appl Energy 2018;212:1191–202.
[6] Strübing D, Moeller AB, Mößnang B, Lebuhn M, Drewes JE, Koch K. Load change capability of an anaerobic thermophilic trickle bed reactor for dynamic H2/CO2 biomethanation. Bioresour Technol 2019;289:121735. https://doi.org/10.1016/j.biortech.2019.121735.
[7] Dupnock TL, Deshusses MA. High-performance biogas upgrading using a biotrickling filter and hydrogenotrophic methanogens. Appl Biochem Biotechnol 2017;183:488–502.
[8] Sieborg MU, Jønson BD, Ashraf MT, Yde L, Triolo JM. Biomethanation in a thermophilic biotrickling filter using cattle manure as nutrient media. Bioresour Technol Rep 2020;9:100391. https://doi.org/10.1016/j.biteb.2020.100391.
[9] Strübing D, Huber B, Lebuhn M, Drewes JE, Koch K. High performance biological methanation in a thermophilic anaerobic trickle bed reactor. Bioresour Technol 2017;245:1176–83.
[10] Strübing D, Moeller AB, Mößnang B, Lebuhn M, Drewes JE, Koch K. Anaerobic thermophilic trickle bed reactor as a promising technology for flexible and demand-oriented H2/CO2 biomethanation. Appl Energy 2018;232:543–54.
[11] Ács N, Szuhaj M, Wirth R, Bagi Z, Maróti G, Rákhely G, et al. Microbial community rearrangements in power-to-biomethane reactors employing mesophilic biogas digestate. Front Energy Res 2019;7:132. https://doi.org/10.3389/fenrg.2019.00132.
[12] Fontana A, Kougias PG, Treu L, Kovalovszki A, Valle G, Cappa F, et al. Microbial activity response to hydrogen injection in thermophilic anaerobic digesters revealed by genome-centric metatranscriptomics. Microbiome 2018;6. https://doi.org/10.1186/s40168-018-0583-4.
[13] Kougias PG, Campanaro S, Treu L, Zhu X, Angelidaki I. A novel archaeal species belonging to *Methanoculleus* genus identified via de-novo assembly and

metagenomic binning process in biogas reactors. Anaerobe 2017;46:23–32. https://doi.org/10.1016/j.anaerobe.2017.02.009.
[14] Basile A, Campanaro S, Kovalovszki A, Zampieri G, Rossi A, Angelidaki I, et al. Revealing metabolic mechanisms of interaction in the anaerobic digestion microbiome by flux balance analysis. Metab Eng 2020;62:138–49. https://doi.org/10.1016/j.ymben.2020.08.013.
[15] Campanaro S, Treu L, Kougias PG, Zhu X, Angelidaki I. Taxonomy of anaerobic digestion microbiome reveals biases associated with the applied high throughput sequencing strategies. Sci Rep 2018;8:1–12.
[16] Treu L, Kougias PG, de Diego-Díaz B, Campanaro S, Bassani I, Fernández-Rodríguez J, et al. Two-year microbial adaptation during hydrogen-mediated biogas upgrading process in a serial reactor configuration. Bioresour Technol 2018;264:140–7. https://doi.org/10.1016/j.biortech.2018.05.070.
[17] Tsapekos P, Kougias PG, Kuthiala S, Angelidaki I. Co-digestion and model simulations of source separated municipal organic waste with cattle manure under batch and continuously stirred tank reactors. Energy Convers Manage 2018;159:1–6. https://doi.org/10.1016/j.enconman.2018.01.002.
[18] Federation WE, Association APH. Standard methods for the examination of water and wastewater. Am Public Health Assoc APHA Wash DC USA 2005.
[19] Bolger AM, Lohse M, Usadel B. Trimmomatic: a flexible trimmer for Illumina sequence data. Bioinformatics 2014;30:2114–20. https://doi.org/10.1093/bioinformatics/btu170.
[20] Li D, Liu C-M, Luo R, Sadakane K, Lam T-W. MEGAHIT: an ultra-fast single-node solution for large and complex metagenomics assembly via succinct de Bruijn graph. Bioinforma Oxf Engl 2015;31:1674–6. https://doi.org/10.1093/bioinformatics/btv033.
[21] Langmead B, Salzberg SL. Fast gapped-read alignment with Bowtie 2. Nat Methods 2012;9:357–9. https://doi.org/10.1038/nmeth.1923.
[22] Li H, Handsaker B, Wysoker A, Fennell T, Ruan J, Homer N, et al. The Sequence Alignment/Map format and SAMtools. Bioinformatics 2009;25:2078–9. https://doi.org/10.1093/bioinformatics/btp352.
[23] Kang DD, Li F, Kirton E, Thomas A, Egan R, An H, et al. MetaBAT 2: an adaptive binning algorithm for robust and efficient genome reconstruction from metagenome assemblies. PeerJ 2019;7:e7359. https://doi.org/10.7717/peerj.7359.
[24] Parks DH, Imelfort M, Skennerton CT, Hugenholtz P, Tyson GW. CheckM: assessing the quality of microbial genomes recovered from isolates, single cells, and metagenomes. Genome Res 2015;25:1043–55. https://doi.org/10.1101/gr.186072.114.
[25] Chaumeil P-A, Mussig AJ, Hugenholtz P, Parks DH. GTDB-Tk: a toolkit to classify genomes with the Genome Taxonomy Database. Bioinformatics 2020;36:1925–7. https://doi.org/10.1093/bioinformatics/btz848.
[26] Hyatt D, Chen G-L, LoCascio PF, Land ML, Larimer FW, Hauser LJ. Prodigal: prokaryotic gene recognition and translation initiation site identification. BMC Bioinf 2010;11:119. https://doi.org/10.1186/1471-2105-11-119.
[27] Shaffer M, Borton MA, McGivern BB, Zayed AA, Rosa SLL, Solden LM, et al. DRAM for distilling microbial metabolism to automate the curation of microbiome function. BioRxiv 2020:2020.06.29.177501. https://doi.org/10.1101/2020.06.29.177501.
[28] Huerta-Cepas J, Szklarczyk D, Heller D, Hernández-Plaza A, Forslund SK, Cook H, et al. eggNOG 5.0: a hierarchical, functionally and phylogenetically annotated orthology resource based on 5090 organisms and 2502 viruses. Nucleic Acids Res 2019;47:D309–14. https://doi.org/10.1093/nar/gky1085.
[29] Galili T, O'Callaghan A, Sidi J, Sievert C. heatmaply: an R package for creating interactive cluster heatmaps for online publishing. Bioinformatics 2018;34:1600–2. https://doi.org/10.1093/bioinformatics/btx657.
[30] Oksanen J, Blanchet FG, Friendly M, Kindt R, Legendre P, McGlinn D, et al. vegan: Community Ecology Package. 2020.
[31] Kanehisa M, Goto S, Sato Y, Kawashima M, Furumichi M, Tanabe M. Data, information, knowledge and principle: back to metabolism in KEGG. Nucleic Acids Res 2014;42:D199–205. https://doi.org/10.1093/nar/gkt1076.
[32] Wickham H. ggplot2. New York, NY: Springer New York; 2009. https://doi.org/10.1007/978-0-387-98141-3.
[33] Rodriguez-R LM, Gunturu S, Harvey WT, Rosselló-Mora R, Tiedje JM, Cole JR, et al. The Microbial Genomes Atlas (MiGA) webserver: taxonomic and gene diversity analysis of Archaea and Bacteria at the whole genome level. Nucleic Acids Res 2018;46:W282–8. https://doi.org/10.1093/nar/gky467.
[34] Kougias PG, Tsapekos P, Treu L, Kostoula M, Campanaro S, Lyberatos G, et al. Biological CO2 fixation in up-flow reactors via exogenous H2 addition. J Biotechnol 2020;319:1–7. https://doi.org/10.1016/j.jbiotec.2020.05.012.
[35] Cresson R, Carrère H, Delgenès JP, Bernet N. Biofilm formation during the start-up period of an anaerobic biofilm reactor—Impact of nutrient complementation. Biochem Eng J 2006;30:55–62.
[36] Cresson R, Dabert P, Bernet N. Microbiology and performance of a methanogenic biofilm reactor during the start-up period. J Appl Microbiol 2009;106:863–76.
[37] Glass J, Orphan VJ. Trace metal requirements for microbial enzymes involved in the production and consumption of methane and nitrous oxide. Front Microbiol 2012;3:61.
[38] Ashraf MT, Sieborg MU, Yde L, Rhee C, Shin SG, Triolo JM. Biomethanation in a thermophilic biotrickling filter — pH control and lessons from long-term operation. Bioresour Technol Rep 2020;11:100525. https://doi.org/10.1016/j.biteb.2020.100525.
[39] Thema M, Weidlich T, Kaul A, Böllmann A, Huber H, Bellack A, et al. Optimized biological CO2-methanation with a pure culture of thermophilic methanogenic archaea in a trickle-bed reactor. Bioresour Technol 2021;333:125135. https://doi.org/10.1016/j.biortech.2021.125135.
[40] Corbellini V, Kougias PG, Treu L, Bassani I, Malpei F, Angelidaki I. Hybrid biogas upgrading in a two-stage thermophilic reactor. Energy Convers Manag 2018;168:1–10. https://doi.org/10.1016/j.enconman.2018.04.074.
[41] Yan M, Treu L, Zhu X, Tian H, Basile A, Fotidis IA, et al. Insights into ammonia adaptation and methanogenic precursor oxidation by genome-centric analysis. Environ Sci Technol 2020;54:12568–82. https://doi.org/10.1021/acs.est.0c0194510.1021/acs.est.0c01945.s002.
[42] Zhu X, Campanaro S, Treu L, Kougias PG, Angelidaki I. Novel ecological insights and functional roles during anaerobic digestion of saccharides unveiled by genome-centric metagenomics. Water Res 2019;151:271–9.
[43] Du Z-J, Wang Z-J, Zhao J-X, Chen G-J. *Woeseia oceani* gen. nov., sp. nov., a chemoheterotrophic member of the order *Chromatiales*, and proposal of *Woeseiaceae* fam. nov. Int J Syst Evol Microbiol 2016;66:107–12. https://doi.org/10.1099/ijsem.0.000683.
[44] Lei Y, Oshima T, Ogasawara N, Ishikawa S. Functional Analysis of the Protein Veg, Which Stimulates Biofilm Formation in Bacillus subtilis. J Bacteriol 2013;195:1697–705. https://doi.org/10.1128/JB.02201-12.
[45] Zhu X, Campanaro S, Treu L, Seshadri R, Ivanova N, Kougias PG, et al. Metabolic dependencies govern microbial syntrophies during methanogenesis in an anaerobic digestion ecosystem. Microbiome 2020;8. https://doi.org/10.1186/s40168-019-0780-9.
[46] Demirel B, Scherer P. The roles of acetotrophic and hydrogenotrophic methanogens during anaerobic conversion of biomass to methane: a review. Rev Environ Sci Biotechnol 2008;7:173–90. https://doi.org/10.1007/s11157-008-9131-1.
[47] Garcia-Robledo E, Ottosen LDM, Voigt NV, Kofoed MW, Revsbech NP. Micro-scale H2–CO2 dynamics in a hydrogenotrophic methanogenic membrane reactor. Front Microbiol 2016;7. https://doi.org/10.3389/fmicb.2016.01276.
[48] McMahon K. Anaerobic codigestion of municipal solid waste and biosolids under various mixing conditions—II: microbial population dynamics. Water Res 2001;35:1817–27. https://doi.org/10.1016/S0043-1354(00)00438-3.
[49] Nguyen LN, Johir MAH, Commault A, Bustamante H, Aurisch R, Lowrie R, et al. Impacts of mixing on foaming, methane production, stratification and microbial community in full-scale anaerobic co-digestion process. Bioresour Technol 2019;281:226–33. https://doi.org/10.1016/j.biortech.2019.02.077.